UCLA
COMPUTATIONAL AND APPLIED MATHEMATICS

Uniform Grid Computation of Smooth Hydrogenic Orbitals

Christopher R. Anderson

February 2015

CAM Report 15-09

Department of Mathematics
University of California, Los Angeles
Los Angeles, CA. 90095-1555

Abstract

In this paper we present a method that can be used to create approximate hydrogenic wave functions that are smooth, have compact support, and which can be accurately represented on a uniform rectangular grid. We investigate the properties of these approximations, and demonstrate that by using appropriate mollification of the nuclear potential one can obtain accurate wave function approximations without excessive refinement of the computational grid near the singularity of the nuclear potential. The accuracy of the wave functions is evaluated by comparison with analytically obtained solutions.

1 Introduction

This paper is concerned with the both the construction and the evaluation of a particular type of approximation of hydrogenic orbitals that are obtained as eigenfunctions of the three dimensional Schroedinger operator in which the nuclear potential is smoothed using high order mollification. The work presented here is motivated by that of [7], where numerically determined orbitals are used to provide atomic centered basis functions for wave-function based methods in quantum mechanics. The specific eigenfunctions considered here are ones that are smooth, have compact support, and can be accurately represented on a uniform rectangular grid. Of particular interest are the computation of those eigenfunctions associated with the algebraically smallest eigenvalues. The desire for orbitals that can be well represented on uniform grids is motivated by the need to determine orbitals for which the one and two electron integrals required for Ab-Initio methods can be evaluated using efficient discrete Fourier transform techniques [3].

As in [7], the principle idea behind the construction of the numerically determined hydrogenic orbitals is to generally follow the "classical" analytical procedure that consists of creating separable eigenfunctions of the Schroedinger operator in spherical coordinates, e.g. $\Psi(r,\theta,\phi) = R(r)\Theta(\theta)\Phi(\phi)$ [6]. The eigenfunctions associated with $\Theta(\theta)$ and $\Phi(\phi)$ components are determined analytically and a finite difference method is used to construct the radial component, $R(r)$. Specifically, in atomic units, the differential operator whose eigenfunctions one seeks is given by

$$-\frac{1}{2}\left[\frac{\partial^2}{\partial x^2}+\frac{\partial^2}{\partial y^2}+\frac{\partial^2}{\partial x^2}+Z/r+V(r)\right]\Psi=\lambda\Psi \tag{1}$$

where $r=\sqrt{x^2+y^2+z^2}$, Z is the nuclear charge and $V(r)$ is an external potential. Assuming wave functions of the form $\Psi(r,\theta,\phi)=R(r)\Theta(\theta)\Phi(\phi)$, then for a given value of l and m (the azimuthal and magnetic quantum numbers) with $l=0,1,2\ldots$ and $m=0\ldots l$ the Θ and Φ components are given by

$$\Phi_{m=0}(\phi)=\frac{1}{\sqrt{2\pi}} \qquad \Phi_m=\frac{\cos m\phi}{\sqrt{2\pi}} \quad \Phi_m=\frac{\sin m\phi}{\sqrt{2\pi}} \qquad \phi\in[0,2\pi] \tag{2}$$

$$\Theta(\theta)=\frac{(2l+1)(l-m)!}{2(l+m)!}P_l^m\cos(\theta) \qquad \theta\in[0,\pi] \tag{3}$$

where P_l^m are the associated Legendre functions [5] defined for $-1\le x\le 1$ by

$$P_l^m=(-1)^m(1-x^2)^{m/2}\frac{1}{2^l l!}\frac{d^{l+m}}{dx^{l+m}}(x^2-1)^l \tag{4}$$

For a given azimuthal quantum number l, the radial components are eigenfunctions defined by

$$\left[-\frac{1}{2}\frac{1}{r^2}\frac{d}{dr}\left(r^2\frac{d}{dr}\right)+\frac{l(l+1)}{r^2}-Z/r+V(r)\right]R(r)=\lambda R(r) \quad r\in[0,\infty] \tag{5}$$

Generally, because of the singular nature of the potential terms, the eigenfunctions of (5) are not smooth. For example, in the case of $V(r)\equiv 0$, analytic eigenfunctions of (5) can be determined [6] and when $l\equiv 0$ the eigenfunctions have a cusp at $r=0$ and when

$l \neq 0$ the eigenfunctions or their higher derivatives have cusps. The presence of the cusps introduces difficulties in the numerical evaluation of integrals involving these eigenfunctions and thus one seeks to determine approximate eigenfunctions (5) that are smooth at $r = 0$. The eigenfunctions of (5) also have infinite extent, a feature that introduces additional difficulties in the numerical evaluation of integrals. One therefore seeks approximations to the eigenfunctions that vanish outside of a prescribed radius as well.

Our procedure for constructing the desired approximate eigenfunctions consists of creating numerically the eigenfunctions of a modified form of (5). In this modified equation a smoothing parameter, ϵ, is introduced to remove the singularity of the potential terms. The eigenfunctions are forced to have compact support through the use of a barrier potential and the introduction of a variable coefficient in the second derivative term. Convergence of the approximate eigenfunctions is obtained in the limit as $\epsilon \to 0$ and the radius of the computational domain increases. The modified equation is described in next section followed by a description of a uniform grid finite difference discretization that can be used to create approximate eigenfunctions of the modified equation. In the last section, computational results that demonstrate the accuracy of the approximations with respect to the mesh size, the smoothing parameter, and computational domain size are presented. In addition, results are presented that demonstrate the accuracy of the three-dimensional eigenfunctions that consist of the products of numerically determined eigenfunctions of (5) with functions given by (2) and (3).

2 The Modified Radial Operator

The singular nature of the potential terms in (5) that induce the non-smooth behavior of the eigenfunctions can accommodated by using approximations that are convolutions of these terms with one of the members of the family of smooth polynomial mollifiers of width ϵ, $B_\epsilon(r)$, given in [2]. These mollifiers have the general form

$$B_\epsilon(r) = \begin{cases} \dfrac{\gamma_q}{4\pi\epsilon^3}\left(1-\left(\dfrac{r}{\epsilon}\right)^2\right)^q \left(1+\displaystyle\sum_{j=1}^{K-1}\alpha_j\left(1-\left(\dfrac{r}{\epsilon}\right)^2\right)^j\right) & r \leq \epsilon \\ \\ 0 & r > \epsilon \end{cases} \tag{6}$$

The values of the coefficients in (6) are determined so that the mollifier has unit L^2 norm in R^3 and has order $2K$. (A mollifier is of order $2K$ if the mollifier has unit mass and all moments from order 1 to $2K$ vanish). The value of q in the mollifier determines its differentiability. For a given value of q, $B_\epsilon(r)$ is $q-1$ times continuously differentiable. The coefficients for mollifiers up to order 6 and up to 9 times continuously differentiable are given in [2]. We mention that the smoothing of the singular terms is determined by convolution in three dimensions with a three dimensional mollifier, not a smoothing based upon the singular terms expressed in radial coordinates and convolved with a one dimensional mollifier.

The determination of expressions for the convolution of the potential terms in (5) with the mollifiers (6) is based upon the observation that $-\dfrac{1}{4\pi r} = G(r)$ where G the fundamental solution of Laplace's equation, e.g. $\nabla^2 G = \delta$ and δ is Dirac's delta function. Thus, letting $*$

denote convolution,

$$-\frac{1}{|\vec{r}|} * B_\epsilon = 4\pi(\nabla^2)^{-1}\delta * B_\epsilon = 4\pi(\nabla^2)^{-1}\mathrm{B}_\epsilon(\vec{r}) = 4\pi\, G_\epsilon \tag{7}$$

where $\nabla^2 G_\epsilon = B_\epsilon$. Since the potential terms in (5) can be expressed as

$$\frac{l(l+1)}{r^2} - Z/r = -l(l+1)\,4\pi\,\frac{dG(r)}{dr} + 4\pi\, Z\, G(r) \tag{8}$$

their mollification can be expressed as

$$\left[\frac{l(l+1)}{r^2} - Z/r\right] * B_\epsilon = -l(l+1)\,4\pi\,\frac{dG_\epsilon(r)}{dr} + 4\pi\, Z\, G_\epsilon(r) \tag{9}$$

As described in [2], if one uses mollifiers of the form (6), then G_ϵ and it's derivatives can be obtained analytically.

Plots of mollifiers of order 2, 4 and 6 with $\epsilon = 1$ are given in Figure 1(a). The mollified Greens' functions, G_ϵ, associated with each of these mollifiers are shown in Figure 1(b) along with the exact Greens' function G. Since the mollifiers B_ϵ vanish outside $r = \epsilon$, the potential terms in (5) are only modified for values $r \leq \epsilon$.

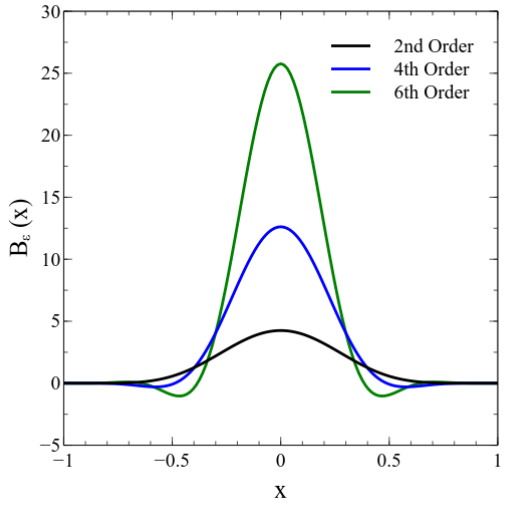

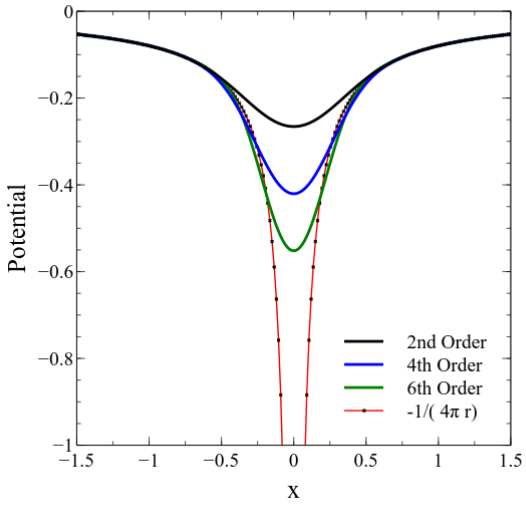

Figure 1(a)

$B_\epsilon(x)$ for $\epsilon = 1$

Figure 1(b)

$G_\epsilon(x)$ for $\epsilon = 1$

To create eigenfunction approximations that vanish for values of $r \geq r_b$, where r_b is the distance to a specified "far-field" boundary, we introduce two modifications of (5). Both modifications make use of a smooth approximation to a Heaviside step function, $s_{\epsilon_b}(t)$, that transitions smoothly from 0 to 1 as t goes from $-\frac{\epsilon_b}{2}$ to $\frac{\epsilon_b}{2}$. Such approximate Heaviside step

functions can obtained by analytically integrating the one dimensional polynomial mollifiers given in [2]. The first modification is to add a "barrier" potential centered at $r = r_b$ with the form

$$V_b(r) = s_{\epsilon_b}(r - r_b)V_\infty \tag{10}$$

This potential vanishes for $r < r_b - \dfrac{\epsilon_b}{2}$ and increases smoothly over a transition distance ϵ_b to a value V_∞. The second modification is to introduce a variable coefficient (a variable reciprocal mass coefficient), $a(r)$, into the second derivative operator,

$$\frac{1}{r^2}\frac{d}{dr}\left(a(r)r^2\frac{d}{dr}\right) \tag{11}$$

where

$$a(r) = 1 - s_{\epsilon_b}(r - r_b) \tag{12}$$

The use of a barrier potential induces the eigenfunctions associated with the algebraically smallest eigenvalues to decay exponentially for $r > r_b$. The use of a variable coefficient that vanishes for $r > r_b + \frac{\epsilon_b}{2}$ insures the eigenfunctions associated with eigenvalues that are less than V_∞ to vanish identically for $r > r_b + \frac{\epsilon_b}{2}$.

With these modifications, the equations whose eigenfunctions are used as approximate eigenfunctions of (5) are given by

$$\left[-\frac{1}{2}\frac{1}{r^2}\frac{d}{dr}\left(r^2a(r)\frac{d}{dr}\right) + 4\pi\, Z\, G_\epsilon(r) + V(r) + V_b(r)\right] R(r) = \lambda R(r) \tag{13}$$

for $l = 0$ and for $l \neq 0$

$$\left[-\frac{1}{2}\frac{1}{r^2}\frac{d}{dr}\left(r^2a(r)\frac{d}{dr}\right) - l(l+1)\,4\pi\,\frac{dG_\epsilon(r)}{dr} + 4\pi\, Z\, G_\epsilon(r) + V(r) + V_b(r)\right] R(r) = \lambda R(r) \tag{14}$$

for $r \in [0, r_b + \dfrac{\epsilon_b}{2}]$. No boundary conditions are specified at $r = 0$ and homogeneous boundary conditions are specified at any value $r > r_b + \frac{\epsilon_b}{2}$.

Alternately, when $l \neq 0$, the non-singular eigenfunctions of (5) vanish at $l = 0$, and one may use

$$\left[-\frac{1}{2}\frac{1}{r^2}\frac{d}{dr}\left(r^2a(r)\frac{d}{dr}\right) - \frac{l(l+1)}{r^2} + 4\pi\, Z\, G_\epsilon(r) + V(r) + V_b(r)\right] R(r) = \lambda R(r) \tag{15}$$

with homogeneous boundary conditions specified at $r = 0$ and any value $r > r_b + \frac{\epsilon_b}{2}$.

In equations (13), (14) and (15) ϵ is the mollifier width associated with the mollification of the singular potential terms. $V_b(r)$ and $a(r)$ depend upon r_b and ϵ_b, the parameters associated with the far-field boundary condition treatment.

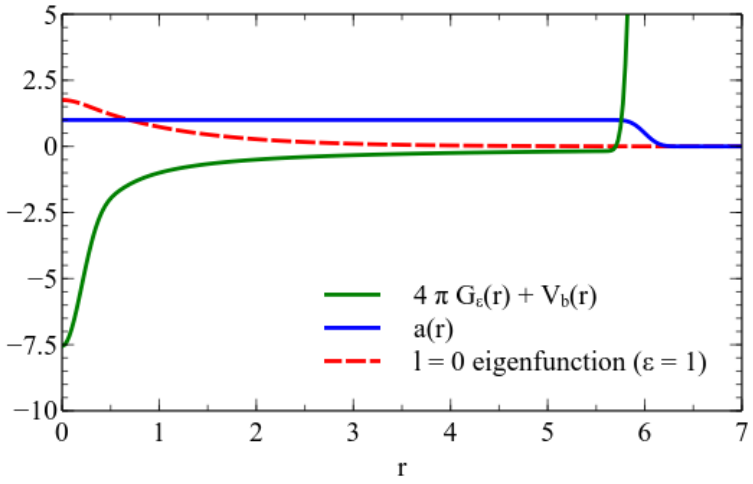

Figure 1: Components of modified radial operator; the sum of the smooth nuclear potential and the barrier potential, $4\pi \mathrm{G}_\epsilon(r) + V_b(r)$; the reciprocal mass coefficient, $a(r)$. The far-field boundary smoothing width $\epsilon_b = 1$.

3 High Order Finite Difference Approximation

To construct a finite difference approximations to (13)-(15) we use a computational domain consisting of an interval $[0, L]$ where $L > r_b + \frac{\epsilon_b}{2}$ and use a uniform grid with mesh width $h = \dfrac{L}{M}$. The grid points are given by $r_i = ih$ for $i = 0 \ldots M$. For equations (13) and (14), even with mollification of the singular potential terms, a primary difficulty in creating high order accurate finite difference approximations is that of creating accurate approximations of the differential operator at $r = 0$ in the presence of the coordinate transformation singularity. The problem associated with the coordinate singularity at $r = 0$ can be avoided by noting that

$$\frac{1}{r^2}\frac{d}{dr}\left(r^2\frac{df}{dr}\right)\bigg|_{r=0} = \left(\frac{d^2f}{dx^2} + \frac{d^2f}{dy^2} + \frac{d^2f}{dx^2}\right)\bigg|_{r=0}, \tag{16}$$

so the evaluation at the origin of the Laplace operator in radial coordinates can be accurately approximated in Cartesian coordinates at the origin using high order centered differences of values along each Cartesian coordinate axis. The assumption that f is a radial function allows one to obtain, without error, the required values along any of the coordinate axis. If one uses a fourth order centered difference approximation, this results in the fourth order approximation

$$\frac{1}{r^2}\frac{d}{dr}\left(r^2\frac{df}{dr}\right)\bigg|_{r=0} = \frac{1}{2}\frac{[-f(2\,h) + 16f(h) - 30f(0)]}{dr^2} \tag{17}$$

Note that we are not making any general assumption about the extension of f to negative values of radial coordinates, e.g. $f(-r) = f(r)$, but only that at $\vec{x} = 0$ in Cartesian coordinates, radial functions $f(r)$ are symmetric in each of the coordinate directions.

At at grid points $r_i > 0$, high order finite difference approximations to the differential operator in (13)-(15) can be obtained by using fourth order finite difference approximations of the individual terms of the equivalent equation

$$a\frac{d^2f}{dr^2} + \frac{a}{r}\frac{df}{dr} + \frac{da}{dr}\frac{df}{dr} \tag{18}$$

Fourth order centered approximations are used when the difference approximations do not require values outside the computational domain, otherwise, non-centered fourth order approximations are used. The requisite coefficients for these finite difference approximations are conveniently tabulated in [1, pg. 918]. The derivatives of a are required for $r > r_b - \frac{\epsilon_b}{2}$. These derivatives can be obtained analytically if one utilizes a smooth step function, $s_{\epsilon_b}(r)$, that is based upon integrating the mollifiers in [2]. Alternately, these derivatives can also be obtained by using fourth order numerical differentiation formulas.

4 Computational Results

4.1 Approximate radial eigenfunctions

In our computational experiments we focused on two representative cases; the algebraically smallest eigenvalues for $l = 0$ and $l = 1$ when $Z = 1$ and $V(x) \equiv 0$. For these cases the eigenfunctions and eigenvalues of the unmodified radial operator (5) are $R(r) = 2\mathrm{e}^{-r}, \lambda = \dfrac{1}{2}$ for $l = 0$ and $R(r) = \dfrac{1}{2\sqrt{6}}\, r\, \mathrm{e}^{-r/2}, \lambda = \dfrac{1}{4}$, for $l = 1$. The eigenfunction associated with $l = 0$ is representative of eigenfunctions that are non-vanishing at $r = 0$ while that associated with $l = 1$ is representative of eigenfunctions that vanish at $r = 0$. Plots of these eigenfunctions are given in Figure 2.

The mesh sized required for the accurate finite difference approximation of the eigenfunctions of (13)-(15) depends upon the size of the mollifier width ϵ. Due to the use of high order finite difference approximations and the smoothness of the solutions being computed, convergence with respect to mesh size is very rapid and typically occurs when the number of panels per ϵ is greater than 8. To insure that the solutions were converged with respect to the mesh size all solutions were evaluated using 18 panels per ϵ. The parameter q associated with the use of the mollifiers (6) determines their differentiability; a value of $q = 9$ was used so that the mollifiers were eight times continuously differentiable. The eigenvalues and eigenvectors of the linear system associated with the finite difference approximation of (13)-(15) were obtained using the Lapack routine GDEEV [4].

Of primary interest is the behavior of the eigenvalues and eigenfunctions of (13)-(15) as the mollifier width ϵ is reduced and the effect of changing the order of the mollifier. A sequence of computations were carried out for values of ϵ from 0.1 to 2.0 with mollifiers of orders 2, 4 and 6. To avoid errors due to finite size domain effects, the far-field parameters were chosen to have values $r_b = 30$, $\epsilon_b = 1$ and $V_\infty = 100$. In Figures 3(a) and 4(a), the absolute difference in the eigenvalue associated with eigenfunctions of (13) and the exact eigenvalues is plotted verses the mollifier width ϵ. In addition to verifying the convergence of the eigenvalues as $\epsilon \to 0$, these results demonstrate that accurate approximations to the

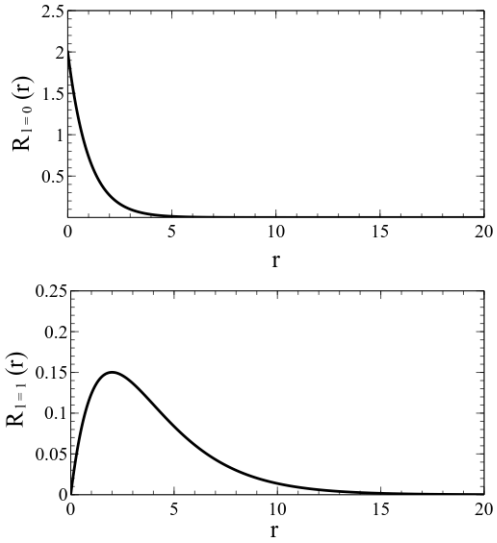

Figure 2: Exact radial eigenfunctions for Z = 1, l = 0 and Z= 1, l = 1.

.

eigenvalues can be obtained even when using rather large values of ϵ. The results also demonstrate the substantial improvement in accuracy that occurs when using high order mollifiers; a sixth order mollifier generally leads to a one to two order of magnitude improvement over computations performed using a second order mollifier. In Figures 3(b) and 4(b) we plot the absolute error in the eigenfunction when $\epsilon = .1, .25, .5$ and 1.0 and a mollifier of order 6. The maximal pointwise error in the eigenfunctions for different values of ϵ is is observed to be localized near the region in which the potential is smoothed.

An interesting aspect of the convergence results is that higher order mollifiers (high order with respect to mollification of the potential) don't necessarily lead to higher order rates of convergence of the eigenvalues. In particular, the slopes of the error curves in Figure 3(a) for 4th and 6th order mollifiers are nearly parallel for small values of the smoothing parameter. This somewhat unsatisfactory aspect is tempered by the observation that even with identical rates of convergence, the high order mollifiers yield much better approximations to the eigenvalues.

In addition to the size of the mollifier width ϵ one must specify the "far-field" components in (13)-(15). The most important parameter of these far-field components is the radial distance r_b, that determines the location of the transition region for the barrier potential, V_b, and the reciprocal mass coefficient $a(r)$. Of interest is the variation of the error in the eigenvalues as this radius is allowed to increase from small to large values. The variation in eigenvalue with respect to this radius is plotted in Figure 5. The behavior shown in this figure confirms the expected; starting with a value of r_b that is much less than the effective radius of the exact eigenfunction leads to a large error in the approximate eigenvalue. As r_b is increased the error decreases monotonically until the value of r_b is equal to effective radius of the eigenfunction. For r_b greater than the effective radius of the eigenfunction, the error

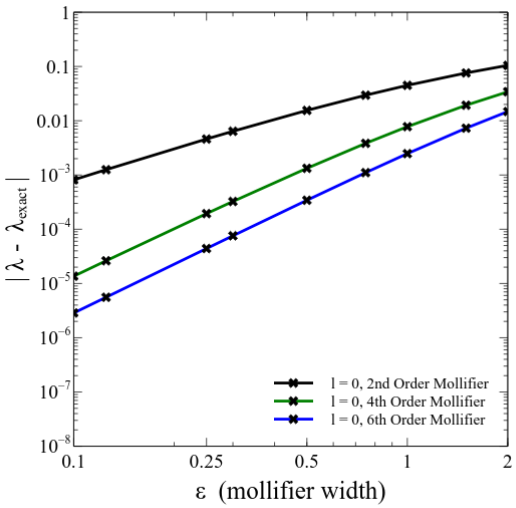

Figure 3(a)
The absolute eigenvalue error
for Z = 1, l = 0.

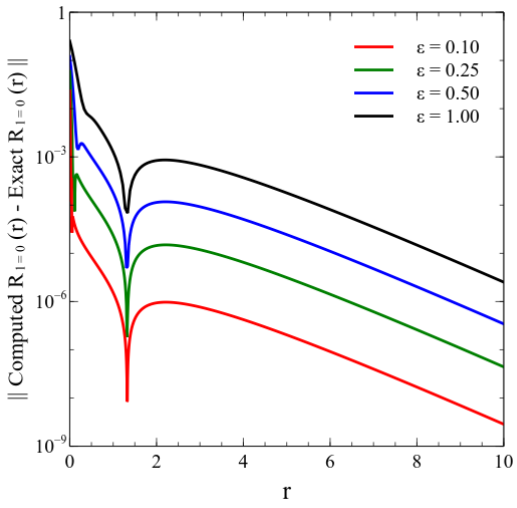

Figure 3(b)
The absolute eigenfunction error for
for Z = 1, l = 0 and mollifier order = 6.

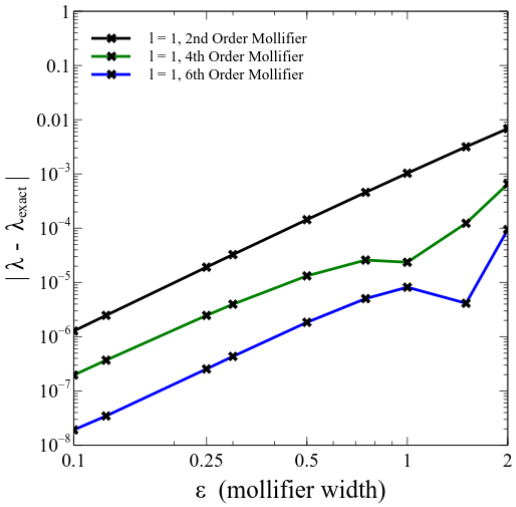

Figure 4(a)
The absolute eigenvalue error
for Z = 1, l = 1.

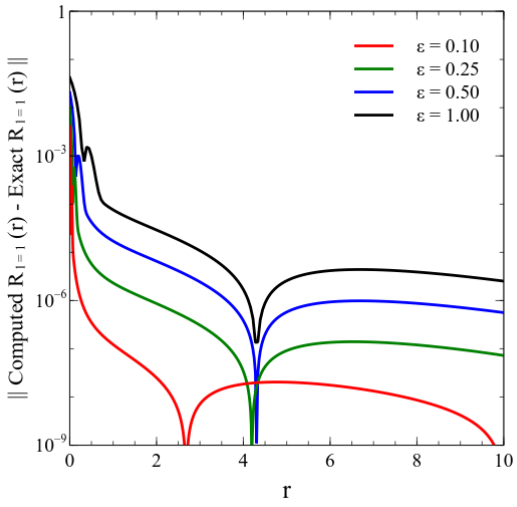

Figure 4(b)
The absolute eigenfunction error
for Z = 1, l = 1 and mollifier order = 6.

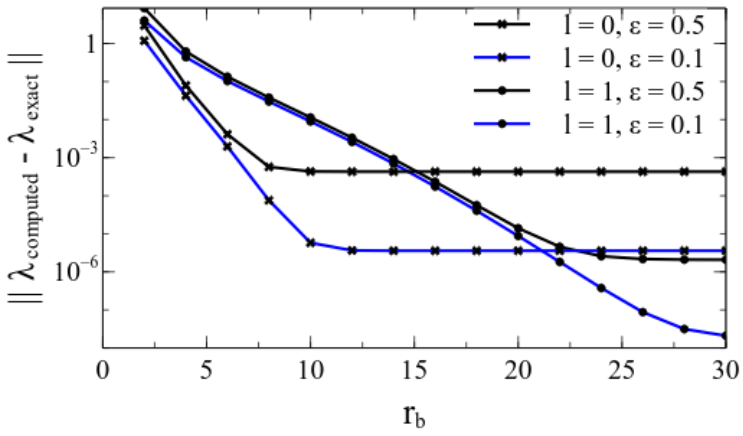

Figure 5: Variation of the absolute eigenvalue error with increasing far-field radius for eigenfunctions with $l = 0, 1$ and $\epsilon = 0.5, 0.1$. Mollifier order = 6.

has a constant value, a value determined by the size of the smoothing parameter ϵ used.

4.2 Approximate three dimensional eigenfunctions

One of the primary motivations for the construction of the radial component of hydrogenic orbitals is their use as the radial components of local atomic centered orbitals (LCAO) basis sets. As mentioned in the introduction, we are interested in classes of local atomic centered orbitals that can be utilized in a computational framework where all computations are carried out using a uniform three dimensional grid. To obtain three-dimensional basis functions on the grid, one solves for the radial component of the eigenfunctions of (13)-(15) with a specified external potential $V(r)$ to obtain the radial component and then multiplies these radial functions by the appropriate spherical harmonics to obtain the θ and ϕ dependence. The values of these basis function are then interpolated to the nodes of a three dimensional grid. Since the principle computation of the basis functions is one-dimensional, these functions are inexpensive to create, and can be obtained with high accuracy. However, there is an error when transferring the basis functions onto the three dimensional grid, and one is interested in the magnitude of this error. Since the principle error is associated with the representation of these functions near the origin, an error that depends significantly on the size of mollifier ϵ, we are particularly interested in this error as a function of the size of ϵ.

One can certainly use the accuracy of the computation of eigenfunctions of (13)-(15) to obtain estimates of the size of the smoothing parameter and minimal mesh size required to obtain a prescribed degree of accuracy of the three dimensional eigenfunctions upon which they are based. However, due to the differences in discretization technique, the fact that the nuclei may not be located at grid points, and that one must use an interpolation of the radial component to construct the three dimensional eigenfunction, the reliability of such estimates is not immediately clear. We therefore carried out a computational investigation

to determine the size of the smoothing parameter and minimal mesh size required to obtain a "maximal error target" of 1.0×10^{-3} for the eigenvalues associated with the full three dimensional eigenfunctions. The computations are performed using atomic units so this "maximal error target" corresponds to an energy error less than a milli-Hartree, or 26 mEV, and is less than the 1 Kcal/mol accuracy known as "chemical accuracy".

To carry out this investigation, a discrete approximation to a modified single-particle three dimensional Schroedinger operator of the form

$$\mathrm{H}\,\Psi = \left[-\frac{1}{2}\nabla^2 - 4\pi G_\epsilon(|\vec{x} - \vec{x}_A|)\right]\Psi = \lambda\Psi \tag{19}$$

was used. In this operator, the nucleus is centered at $\vec{x}_A$ and $G_\epsilon(\vec{x})$ is a smoothed fundamental solution of the Laplace equation obtained by mollification with 6th order mollifier of radius ϵ. The size of the smoothing parameter ϵ was taken to be identical to that used when determining the eigenfunctions of (13)-(15) for the radial component. A rectangular computational domain $[-L, L] \times [-L, L] \times [-L, L]$ was used with $L > r_b + \frac{\epsilon_b}{2}$, where r_b and ϵ_b were the far-field parameters used in the construction of solutions to(13)-(15). In the operator (19), no special handling of the far-field is required since the eigenfunctions to which this operator is applied has compact support. Fourth and sixth order, symmetric, centered, finite difference approximations were used in the discretization of ∇^2.

The nuclear center was located at $\vec{x}_A = (.1, .3, .2)$, e.g. not centered on a grid node. For the $l = 0$ eigenfunction, a domain width $L = 10$ was used, and for the $l = 1$ eigenfunction, $L = 20$ was used. The eigenvalues were evaluated using the Rayleigh quotient, $\lambda = \dfrac{\langle \mathrm{H}\,\Psi, \Psi\rangle}{\langle \Psi, \Psi\rangle}$, with standard trapezoidal method approximation to the integrals required for the evaluation of the inner products.

In Figure 6(a) and 6(b) we show the absolute errors in eigenvalues associated with the approximate three dimensional eigenfunctions with quantum indices $n = 1, l = 0, m = 0$ and $n = 2, l = 1, m = 0$ as a function of the number of grid panels per atomic unit (au). The dashed line in the figures indicates the "maximal error target".

The expected need for a finer three-dimensional grid spacing as ϵ is reduced is clearly apparent. However, an excessively small mesh is not needed, in fact, these results reveal that target accuracy can be achieved for the $l = 0$ case using a rather large smoothing parameter of $\epsilon = .5$ and a mesh size of 6 panels per atomic unit. Moreover, for the eigenfunctions with $l \neq 0$, the smoothing parameter can be very large and one can use a very coarse grid. This result is not surprising in light of the fact that the eigenfunctions with $l \neq 0$ vanish at the origin, and thus the eigenfunction isn't as strongly influenced by the mollification of the potential in the neighborhood of the origin.

5 Conclusion

We have presented a method for construction of the radial component of hydrogenic eigenfunctions that are smooth and are of compact support. The numerical computation of this radial component uses high order finite difference discretizations on a uniform mesh. The singular potential terms in the equation determining the radial components are accommodated by replacing them with smoothed (mollified) approximations to the three dimensional

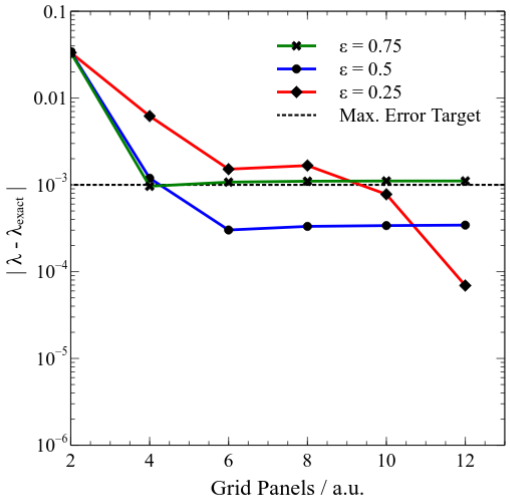

Figure 6(a)

The absolute eigenvalue error for $N = 1, l = 0, m = 0$. $\lambda_{exact} = \frac{1}{2}$.

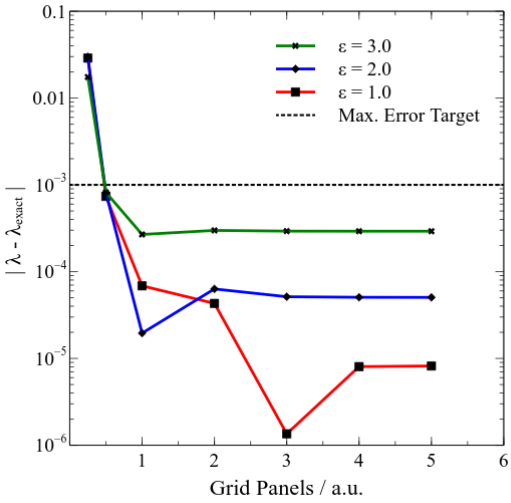

Figure 6(b)

The absolute eigenvalue error for $N = 2, l = 1, m = 0$. $\lambda_{exact} = \frac{1}{8}$.

potential and it's derivatives. The "far-field" behavior is accommodated using a combination of a barrier potential and a variable reciprocal mass coefficient. The computational results demonstrate that with rather large values of the potential smoothing parameter and without excessive grid refinement one can achieve accurate approximations to both the eigenvalues and eigenvectors of the un-modified Schroedinger equation. The computational results also reveal that the use of higher order mollifiers is extremely beneficial, typically resulting in a one to two order magnitude improvement in accuracy over the use of second order mollifiers.

The eigenfunctions of the modified radial operator can be used to form approximate three-dimensional eigenfunctions. These eigenfunctions are constructed as products of functions of spherical coordinates where the radial components is computed numerically and the remaining components (spherical harmonics) are evaluated analytically. The computational experiments indicate that when these functions are evaluated on the nodes of a three dimensional grid, the resulting discrete eigenfunctions are good approximations to the eigenfunctions of the three-dimensional Schroedinger operator, and that "chemical accuracy" can be obtained without excessively fine grids.

While we have concentrated on the determination of eigenfunctions associated with the Schroedinger operator where the potential is a nuclear potential, the finite difference method is certainly applicable to more general radial potentials. Thus, the procedure may be of value in investigations similar to that in [7], where eigenfunctions associated with different potentials are use to create improved basis sets for methods based on density functional theory. We also mention that the discretization ideas associated with mollification of the nuclear potential and handling of far-field boundaries are readily generalized to methods for the creation of approximate of eigenfunctions used as a basis for poly-atomic systems [3].

Bibliography

[1] Milton Abramowitz and Irene A. Stegun. *Handbook of Mathematical Functions with Formulas, Graphs, and Mathematical Tables*. Dover, ninth dover printing, tenth gpo printing edition, 1964.

[2] Christopher R. Anderson. Compact Polynomial Mollifiers For Poisson's Equation. Technical Report CAM-14-43, Department of Mathematics, UCLA, Los Angeles, California, May 2014.

[3] Christopher R. Anderson. Grid Based Solutions of the N-Particle Schroedinger Equation. Technical Report CAM-15-10, Department of Mathematics, UCLA, Los Angeles, California, February 2015.

[4] E. Anderson, Z. Bai, C. Bischof, S. Blackford, J. Demmel, J. Dongarra, J. Du Croz, A. Greenbaum, S. Hammarling, A. McKenney, and D. Sorensen. *LAPACK Users' Guide*. Society for Industrial and Applied Mathematics, Philadelphia, PA, third edition, 1999.

[5] N.N. Lebedev and R.A. Silverman. *Special Functions and Their Applications*. Dover Books on Mathematics Series. Dover Publications, 1972.

[6] L. Pauling and E.B. Wilson. *Introduction to Quantum Mechanics With Applications to Chemistry*. Dover Books, 1935.

[7] Igor Ying Zhang, Xinguo Ren, Patrick Rinke, Volker Blum, and Matthias Scheffler. Numeric atom-centered-orbital basis sets with valence-correlation consistency from H to Ar. *New Journal of Physics*, 15(12):123033, 2013.